APL Materials

Magnetic vortex evolution in self-assembled $La_{0.7}Sr_{0.3}MnO_3$ nanoislands under in-plane magnetic field

Cite as: APL Mater. **2**, 076111 (2014); https://doi.org/10.1063/1.4891277
Submitted: 04 April 2014 . Accepted: 15 July 2014 . Published Online: 28 July 2014

J. Zabaleta, M. Jaafar, A. Asenjo, S. Agramunt-Puig, N. Del-Valle, C. Navau, A. Sanchez, T. Puig, X. Obradors, and N. Mestres

Magnetic vortex evolution in self-assembled $La_{0.7}Sr_{0.3}MnO_3$ nanoislands under in-plane magnetic field

J. Zabaleta,[1,a,b] M. Jaafar,[2] A. Asenjo,[2] S. Agramunt-Puig,[3] N. Del-Valle,[4] C. Navau,[4] A. Sanchez,[4] T. Puig,[1] X. Obradors,[1] and N. Mestres[1,b]
[1]*Institut de Ciència de Materials de Barcelona, ICMAB-CSIC, Campus de la UAB, 08193 Bellaterra (Barcelona), Catalonia, Spain*
[2]*Instituto de Ciencia de Materiales de Madrid, ICMM-CSIC, Sor Juana Inés de la Cruz 3, Cantoblanco, 28049 Madrid, Spain*
[3]*Group of Smart Nanoengineered Materials, Nanomechanics and Nanomagnetism, Universitat Autònoma Barcelona, 08193 Bellaterra (Barcelona), Catalonia, Spain*
[4]*Grup d'Electromagnetisme, Departament de Física, Universitat Autònoma de Barcelona, 08193 Bellaterra (Barcelona), Catalonia, Spain*

(Received 4 April 2014; accepted 15 July 2014; published online 28 July 2014)

The magnetic vortex formation at room temperature and its evolution under in-plane magnetic field is studied in chemically grown self-assembled $La_{0.7}Sr_{0.3}MnO_3$ nanoislands of less than 200 nm in width. We use variable field magnetic force microscopy and numerical simulations to confirm that the vortex state is ubiquitous in these square-base pyramid shape epitaxial $La_{0.7}Sr_{0.3}MnO_3$ nanostructures, and that it requires in-plane magnetic fields below 40 kA/m to be annihilated. [http://dx.doi.org/10.1063/1.4891277]

Nanoscale magnetism is of great scientific interest and high technological relevance.[1,2] As a consequence, many research efforts have been devoted during the past few years to the design and growth of nanostructures of magnetic materials in order to investigate the size reduction effects on their functionality and potential applications, with the perspective of integrating them into devices. The primary functions of such devices are essentially determined by the local magnetic moment orientation, which in turn is established by the size and shape of the ferromagnetic objects. Designed magnetic structures with dimensions in the submicrometer scale exhibit a specific magnetic ordering, including magnetic vortices.[3–5] A growing interest on magnetic vortices arose as the improved sensibility of imaging techniques allowed to observe the vortex core[5,6] and made accessible its internal structure.[7] In fact, the vortex core has become an appealing memory unit candidate for data storage[8,9] and, also recently, various types of emerging devices such as microwave oscillators[10,11] and amplifiers[12,13] based on the properties of magnetic vortices were proposed.

In metal-based magnetically soft nanostructures like permalloy, shape anisotropy is the main ingredient determining the magnetic ground state. However, the superposition of a biaxial anisotropy to the shape anisotropy may have a determinant influence in stabilizing the magnetic ground state.[14,15] A good candidate for nanoscale-based magnetic applications is nanostructures of the mixed-valence manganite $La_{0.7}Sr_{0.3}MnO_3$ (LSMO), a complex oxide that exhibits high spin polarization and colossal magnetoresistance, and biaxial magnetocrystalline anisotropy.[16,17] However, it has been shown that in manganite systems magnetic anisotropy could be a complex issue, and depending on the exact film-substrate characteristics, the level of tensile or compressive strain, thickness, or temperature, either the biaxial or uniaxial anisotropy dominates the magnetic behavior.[18]

Cost-effective fabrication methods to produce organized arrays of functional oxide nanostructures on substrates are in demand due to the potential applications of these materials in the next

[a]Present address: MPI-FKF Heisenbergstrasse 1, 70569 Stuttgart, Germany.
[b]Electronic addresses: j.zabaleta@fkf.mpg.de and narcis.mestres@icmab.es

generation of devices. Top-down procedures are the methods that nowadays offer excellent control of shape and arrangement of nanostructures.[19–21] The patterning of complex oxide materials however has been sometimes challenging due to the inherent chemical stability and refractory nature of many oxides. Also, cost and scalability is under discussion in some situations. In this context, strong effort is being pursued with alternative methods using bottom-up self-assembly and assisted self-assembling approaches based on chemical solution processes which should prove to be able to produce nanostructures of small lateral size and narrow size distribution. Although nowadays they are in a pre-competitive stage, these new routes may constitute a promising route to functional oxides nanostructuration in the future. Therefore, understanding the properties and behavior of self-assembled oxide nanostructures is already a need. Chemical methods have already been proved efficient in producing high quality epitaxial thin films, 0D and 1D nanostructures.[22–24]

In their 2002 paper, Okuno and co-workers revealed the stability of magnetic vortices in circular permalloy dots of diameter D and thickness t subject to out-of-plane applied magnetic fields.[25] Their measurements for constant thickness dots of different aspect ratios ($D/t = 4$, 8, and 20) showed that the necessary field to switch the vortex core was as large as ∼325 kA/m, and did not depend on the lateral size of the dot, proving that the core is an independent entity within the surrounding in-plane magnetic structure. By contrast, the evolution of the vortex state under in-plane magnetic field offers wider possibilities with much smaller fields involved. It is well known that the magnetization reversal under an in-plane applied magnetic field proceeds via vortex nucleation, displacement, and annihilation.[4,9] The new ground state is no longer the centered vortex state but a new state, now stabilized by the Zeeman contribution.

In our recent work,[26,27] we have described the rich variety of magnetic structures adopted by solution-derived self-assembled LSMO nanoislands, a system with intrinsic biaxial magneto-crystalline anisotropy in contrast to the more common permalloy nanodots. In particular, we showed that the vortex state is the preferred configuration for a broad range of LSMO nano-sized geometries. X-ray magnetic circular dichroism (XMCD) imaging performed at low temperatures (110 K) in remanence and under in-plane magnetic field evidenced the formation and evolution of vortices in both squared (001)- and triangular (111)-oriented LSMO nanoislands. Towards their use as building blocks in real devices, it is now of great interest to study the room temperature stability of these LSMO vortices and their behavior under an externally applied in-plane magnetic field. The implementation of magnetic nanostructures in modern applications requires knowing, for instance, under what fields the configuration is stable and when it switches magnetization. In the present work, we present a magnetic force microscopy (MFM) study of the nanoscale magnetic structure of solution-derived self-assembled LSMO nanoislands under an in-plane applied magnetic field reaching values up to 36 kA/m. We additionally perform numerical simulations that take into account realistic parameters of these islands in order to understand the formation and evolution of the vortices.

We prepared self-assembled LSMO nanostructures on top of yttria-stabilized zirconia (YSZ) single crystals using a chemical route described previously.[26] In the samples we study here two types of nanoislands were present: square-base truncated pyramid nanoislands (∼80%), which show a (001)LSMO[110]//(001)YSZ[100] epitaxial arrangement, and triangle-base nanoislands (∼20%), with the (111)LSMO[-112]‖(001)YSZ[100] arrangement. Both types of islands show good crystallinity, are faceted, and strain-relaxed.[26,27] Nanoislands display lateral sizes D between ∼40 and 180 nm and thickness values t between ∼10 and 40 nm.

The MFM measurements were done using a variable field magnetic force microscope (VF-MFM), adapted from a commercial AFM from Nanotec Electrónica S.L., and working at room temperature. A detailed description of the system is given in Ref. 28. Our main goal is to study the micromagnetic structure of individual islands and to see how their magnetic domain configuration varies under in-plane magnetic field. The set-up we used consists of a copper electromagnet (0.5 mm diameter wire) connected to two iron bars that enclose the magnetic flux created by the coil and that are separated by an air gap. The sample is located between the ends of the iron pieces and the field intensity can be changed by changing their separation (between 4 and 8 mm). In our case, maximum fields of ∼36 kA/m were reached when applying a 2 A current flow through the coil. The current to field calibration was done systematically before a series of measurements was undertaken. MFM imaging was performed in the dynamic mode using the lift-mode operation, i.e., the oscillating

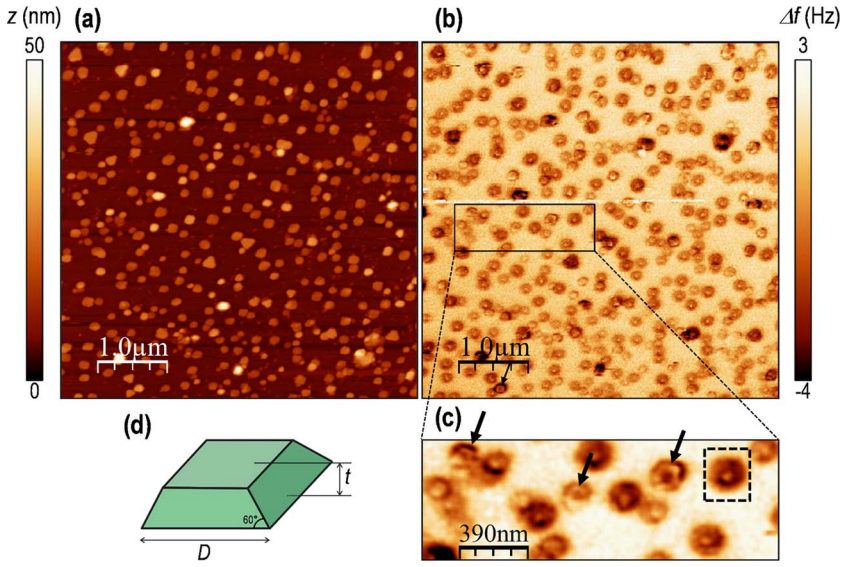

FIG. 1. (a) Topography image and (b) the corresponding MFM map of a sample of self-assembled LSMO nanoislands. The vast majority of the islands in (b) show a contrast characteristic of a vortex state configuration, and most of them display a core pointing outwards (bright contrast). (c) Some of the vortices with the core pointing downwards (dark contrast in the core) are signaled by black arrows in the zoomed area below. (d) Sketch of the square-base truncated pyramid morphology that the majority of islands show, such as the one within a dashed square in (c).

cantilever (free amplitude ∼8 nm) was placed at two different distances from the sample surface for each scanned line: close to the surface (∼5 nm) first, for topography data acquisition, and far from the surface afterwards, for the magnetic signal collection, at typical retrace distances of 30–60 nm. During the retrace the previous topography movements are repeated in order to exclude topography effects in the magnetic signal. We measured using the phase locked loop (PLL) feedback activated, which, by keeping the phase of the oscillation constant, ensures that the topography channel purely reflects Van der Waals interactions. The magnetic interaction is then detected by measuring the frequency shift required to keep the phase constant. Accordingly, an increase in frequency, imaged as a bright contrast, stands for a repulsive interaction between tip and sample, and a dark contrast stands for an attractive interaction.

Magnetic tips are saturated using a permanent magnet prior to imaging the sample. The tip is magnetized parallel to its axis, that is, perpendicular to the sample surface, which is done easily because of its large shape anisotropy. We have verified that the successful imaging of the system relies on the adequate tuning of the experimental conditions, and, specifically, on the appropriate choice of the magnetic tip. A commercial ∼40 nm CoCr coated tip (PPP-MFMR from Nanosensors) was found to be the best compromise between sensitivity and sample modification, revealing a clear magnetic signal arising from the LSMO nanoislands.

Macroscopically, the epitaxial LSMO nanoisland ensemble showed ferromagnetic behavior with a Curie temperature $T_c \sim 350$ K, as measured by Superconducting Quantum Interference Device (SQUID) magnetometry. Saturation magnetization (M_s) values at $T = 35$ K were a 10%–30% lower than the 590 kA/m value of bulk LSMO (3.7 μ_B per Mn atom). At room temperature, the M_s of the island ensemble decreases to values between 260 kA/m and 300 kA/m, depending on the sample.[26] X-ray absorption spectra (XAS) showed bulk like composition and Mn^{2+} rich surfaces, which may account for the loss in magnetization measured by SQUID magnetometry.[27]

Figures 1(a) and 1(b) show the topography and the corresponding magnetic signal image, respectively, of the self-assembled LSMO nanoislands in remanence. The MFM image was taken after saturating the sample *ex situ* with a 400 kA/m field applied perpendicular to the sample substrate, and in the direction opposite to the tip stray field. A clear contrast arises from the islands as a result of the magnetic interaction between the islands and the tip of the MFM. Nanoislands

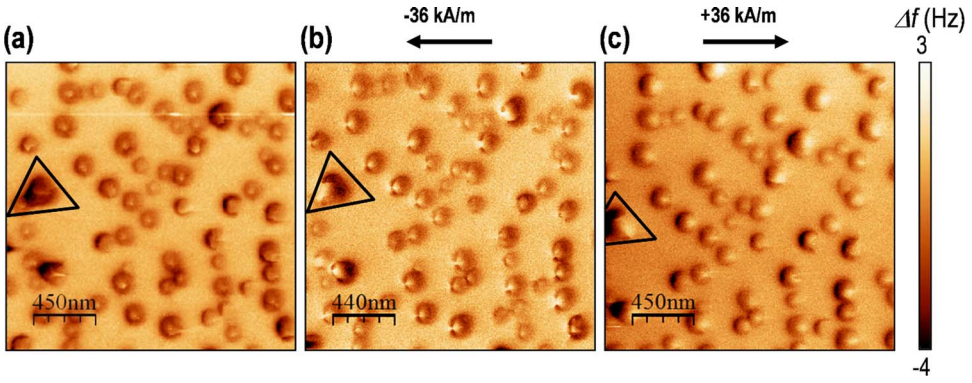

FIG. 2. (a) MFM image of self-assembled LSMO nanoislands taken in remanence after saturating tip and islands in out-of-plane and opposite directions. (b) & (c) MFM images of the same region under ∼36 kA/m external field applied parallel to the substrate edge, which coincides with the horizontal MFM image frame. A large triangular nanoisland is marked in every image for reference.

display lateral sizes D between ∼40 and 180 nm and thickness values t between ∼10 and 40 nm. In the MFM image of Fig. 1(b), the vast majority of the islands show a bright spot close to the center, and they can be identified as vortices with their core pointing outwards. The predominance of bright spots is due to the prior *ex situ* saturation, where the islands are first magnetized opposite to the tip (i.e., repulsively interacting with the tip, thus exhibiting bright contrast). When the field is turned off, the island relaxes into the in-plane curling vortex state, with its core pointing preferably outwards, and only very few show the opposite core orientation (Fig. 1(c) and Figure S1 of the supplementary material[29]). The dark contour, which reveals an attractive interaction surrounding the bright core, can be explained as a combination of two effects: for one side, the stray field from the magnetic tip tilts slightly the in-plane curled moments towards a parallel alignment and, for the other, the contrast arising from the 90° domain walls in such small structures cannot be resolved with the MFM lateral resolution and may give rise to a blurred contrast.[30,31] Although much fewer, some vortices with the core pointing downwards can also be observed (see Fig. 1(c)). The detection of the two energetically equivalent *up* and *down* states is yet another evidence of the vortex state in which these LSMO nanoislands arrange, in this case at room temperature and using a technique which is mainly sensitive to the core of the vortex.

Figure 2 shows how the configuration of the system changes when imaged under in-plane magnetic field. The centered vortices of the remanence state (Fig. 2(a)) evolve into a very different state when we applied our maximum reachable magnetic field, 36 kA/m, in two opposite directions (Figs. 2(b) and 2(c)). A black triangle on the left side serves as reference for identifying individual islands in the three images (thermal drift causes position to slightly vary during successive scans).

Fig. 3 gives a closer view of selected islands which are representative examples of how LSMO nanoislands behave under in-plane magnetic field. Two regions, labeled 1 and 2, are marked with white squares in the topography image at the top of the figure. Zoomed-in magnetic contrast images of such regions are shown below, along with their topography (top half of the profile) and MFM line scans (bottom half of the profiles). The **vortex-state** (V) featured by a square-base truncated pyramid in region 1 shows a bright core at 0 kA/m applied field (see also the line scan), and a dipolar bright-dark contrast under 36 kA/m, characteristic of a saturated single domain state.[32,33]

The dipolar contrast is very clear at 36 kA/m, whereas at −36 kA/m it has a horse-shoe like structure, most probably due to the presence of a slight remanent field at zero applied current, which causes the effective field in both directions not to be identical. The small island in between two islands in region 1 is an example of a low-contrast island, of the type which is at the limit of sensitivity of our equipment, and which we know from micromagnetic simulations to display a **single-domain** (SD) structure.[27] Indeed, its weak magnetic contrast, less than 1 Hz in magnitude, shows no observable structure change when imaging at different magnetic fields. Region 2 gathers a series of vortices in square-based truncated islands and also a **triangular** (111)-LSMO island.

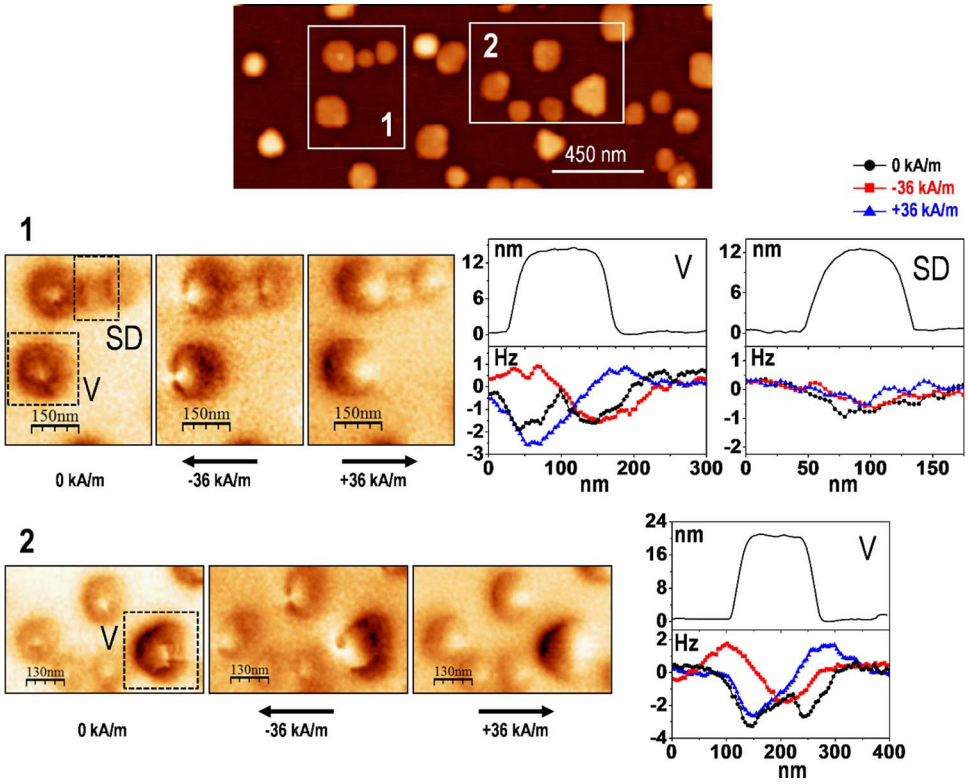

FIG. 3. (Top) Topography image of LSMO nanoislands (z scale 45 nm). (Bottom) Magnetic signal images of the islands in region 1 and 2 in remanence, and under in-plane field. Region 1 shows a vortex (V) in remanence and its saturated state (monodomain showing dipolar contrast) at in-plane fields of ±36 kA/m. A single domain (SD) island barely gives any contrast. Region 2 shows the vortex and the single-domain saturated state under applied field for a triangular island. The topography and magnetic contrast line scans of the selected islands are shown on the right side.

The remanence image of the triangle evidences the stabilization of a magnetic vortex state in (111) oriented triangular LSMO nanoislands, and confirms the previous results obtained by XMCD at low temperatures.[27] While XMCD is most sensitive to magnetization in the plane of the sample, MFM is primarily sensitive to the out-of-plane magnetization component of the magnetic stray field of the sample.

The detailed evolution of the magnetic configuration of a square-based pyramidal LSMO nanoisland ($D = 155$ nm, $t = 14$ nm) under sequential in-plane magnetic fields, is shown in Figure 4. We observe that field values below 36 kA/m yield slightly off-centered vortices. The intermediate states between −36 kA/m and 36 kA/m reveal the displacement of the vortex core, from the aforementioned horse-shoe structure to that of the saturated nanoisland. The change in the location of the core apex changes imperceptibly for fields in between −16 kA/m and 16 kA/m. This is not unexpected, since the lateral MFM resolution, around 50 nm, does not allow resolving the exact location of the core. The fact that the vortex core shifts position with changing magnetic field is a clear signal that the structure of the core is rearranging under the influence of the field. However, because of the convolution between the magnetic tip and sample, this movement cannot be resolved.

The formation of magnetic vortices in strain-relaxed LSMO nanoislands with a truncated square-base pyramidal shape seems ubiquitous, as proved using two different techniques (PEEM[27] and MFM). In order to confirm our experimental results from a theoretical viewpoint and to shed light into the evolution of these vortices within the range of the applied magnetic fields, we next performed numerical simulations (using a self-built code) of the magnetization of such LSMO nanoislands.

We calculated the magnetization distribution of a square-base truncated pyramid nanoisland with its base on the xy plane (side of the base $D = 144$ nm and thickness $t = 24$ nm) by using our own micromagnetic code based on iteratively solving Brown's equations,[34] in which the

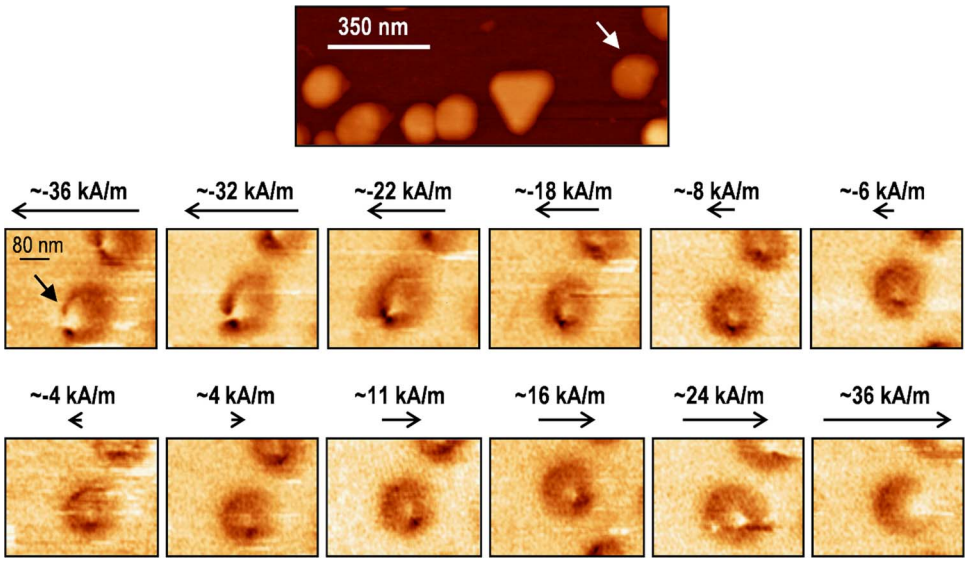

FIG. 4. Evolution of the magnetic contrast of a LSMO nanoisland under in-plane magnetic field. The island is shown in the topography image above (z scale 45 nm). MFM can barely resolve the variations that drive each island from a saturated monodomain to a vortex and back to a monodomain state again.

exchange, magnetostatic, Zeeman, and uniaxial anisotropy interactions are considered. We have used a saturation magnetization $M_s = 386$ kA/m, an exchange constant $A = 1.73 \times 10^{-12}$ J/m, and a magnetocrystalline anisotropy $K_1 = 5.0 \times 10^3$ J/m^3.[26] The truncated pyramid is discretized into a uniform array of cubic cells of side 4 nm according to the exchange length ($l_{ex} = \sqrt{2A/\mu_0 M_s^2} \approx 4.3$ nm). When the magnetization distribution is found we calculate the global sample magnetization as the addition of the contribution of all cells, and also the stray magnetic field (and its derivatives) at any point of the exterior space. In particular, we calculate the second derivative of the field with respect to z at a height $z = t + 30$ nm, which would correspond to the position of the MFM magnetic tip. In such way, we obtain a map in the xy plane whose qualitative trend can be compared to the MFM results, since the magnetic contrast measured by MFM is also proportional to the second derivative of the field. Note, however, that the calculations show a derivative at a point, whereas a MFM image spot would correspond to a certain average of that derivative in a given region. Using this procedure, we have calculated the magnetization loop of the x-component of the magnetization as a function of the applied field $M_x(H_a)$ (Fig. 5-center). Starting with a large positive applied field and reducing it to zero, the magnetization distribution is first practically uniform in the applied field direction (Fig. 5(h)) and the MFM scan would show the characteristic dipolar bright-dark contrast (Fig. 5(d)). When the field is further reduced (making it negative) a C-state starts to form (Fig. 5(g)) and a strong contrast in the MFM image in one side of the pyramid appears (Fig. 5(c)). Further decreasing the applied field finally leads to a vortex state with a core down (Fig. 5(f)) producing a "quadrupolar" bright-dark contrast and a black spot (vortex core) in the MFM image (Fig. 5(b)). The vortex is formed out of the center because of the coercivity of the nanoisland. Thus, a relatively small decrease (increase of negative) of the applied field results in the annihilation of the vortex around 23 kA/m and the nanoisland returns to a uniform state (Figs. 5(e) and 5(a)). Our model can qualitatively explain the MFM maps and it is useful to study the vortex creation and annihilation in the nanoislands, see Figure S2 of the supplementary material.[29] We have shown, in particular, that for this geometry and material parameters the field of annihilation of the vortex is in reasonable agreement with the experiments.

This work shows the presence and evolution of magnetic vortices at room temperature in strain-relaxed epitaxial LSMO nanoislands below 200 nm in lateral size. VF-MFM imaging of these islands is able to clearly detect the vortex core and their saturation state. The latter requires an in-plane magnetic field in the order of 36 kA/m, an easily achievable magnetic field an order of

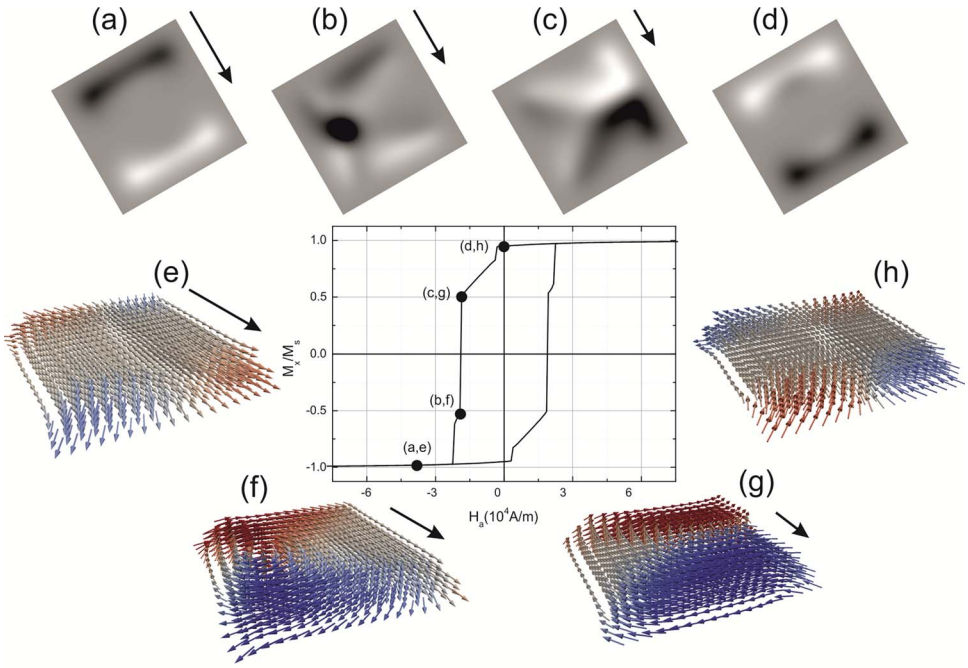

FIG. 5. (Center) Calculated magnetization loop for a square-base truncated pyramidal LSMO nanoisland under in-plane applied field. (a)–(d) Maps of the second derivative of the field produced by the magnetization distribution (arbitrary units) at a certain distance (30 nm) from the top of the pyramid. Different maps correspond to different applied fields as shown in the magnetization loop. (e)–(h) Sketch of the magnetization distribution at different applied fields during the loop, the number of arrows is reduced in this plot for clarity. Colors in arrows indicate the magnitude of the *y* component of the magnetization, red being positive and blue negative. The applied field direction is parallel to the island facet and its sense is indicated by black arrows.

magnitude below the reported out-of-plane fields necessary to switch the vortex core magnetization. Numerical simulations tailored to the characteristics of these LSMO nanoislands not only confirm the formation of the vortex state and the range of the vortex annihilation fields, but also reveal the intermediate magnetization states, which are hidden in the MFM study by the small island-finite MFM tip convolution.

Financial support from Spanish MICINN (MAT2011-29874-C02-01, Consolider: NANOSELECT CSD2007-00041 and CSD2010-00024), and Generalitat de Catalunya (2009 SGR 770 and Xarmae) are acknowledged. J.Z. acknowledges FPU Ph.D. grant from Spanish MICINN.

[1] K. J. Kirk, Contemp. Phys. **41**, 61 (2000).
[2] S. D. Bader, Rev. Mod. Phys. **78**, 1 (2006).
[3] R. P. Cowburn, D. K. Koltsov, A. O. Adeyeye, M. E. Welland, and D. M. Tricker, Phys. Rev. Lett. **83**, 1042 (1999).
[4] K. Y. Guslienko, V. Novosad, Y. Otani, H. Shima, and K. Fukamichi, Phys. Rev. B **65**, 024414 (2001).
[5] T. Shinjo, T. Okuno, R. Hassdorf, K. Shigeto, and T. Ono, Science **289**, 930 (2000).
[6] K. Yamada, S. Kasai, Y. Nakatani, K. Kobayashi, H. Kohno, A. Thiaville, and T. Ono, Nat. Mater. **6**, 270 (2007).
[7] A. Wachowiak, J. Wiebe, M. Bode, O. Pietzsch, M. Morgenstern, and R. Wiesendanger, Science **298**, 577 (2002).
[8] B. Pigeau, G. De Loubens, O. Klein, A. Riegler, F. Lochner, G. Schmidt, L. W. Molenkamp, V. S. Tiberkevich, and A. N. Slavin, Appl. Phys. Lett. **96**, 132506 (2010).
[9] R. P. Cowburn, J. Magn. Magn. Mater. **242–245**, 505 (2002).
[10] A. Ruotolo, V. Cros, B. Georges, A. Dussaux, J. Grollier, C. Deranlot, R. Guillemet, K. Bouzehouane, S. Fusil, and A. Fert, Nat. Nanotech. **4**, 528 (2009).
[11] V. S. Pribiag, I. N. Krivorotov, G. D. Fuchs, P. M. Braganca, O. Ozatay, J. C. Sankey, D. C. Ralph, and R. A. Buhrman, Nat. Phys. **3**, 498 (2007).
[12] T. Nozaki, H. Kubota, S. Yuasa, M. Shiraishi,T. Shinjo, and Y. Suzuki, Appl. Phys. Lett. **95**, 022513 (2009).
[13] S. Kasai, K. Nakano, K. Kondou, N. Ohshima, K. Kobayashi, and T. Ono, Appl. Phys. Exp. **1**, 091302 (2008).
[14] D. B. Carlton, N. C. Emley, E. Tuchfeld, and J. Bokor, Nano Lett. **8**, 4173 (2008).
[15] E. J. Kim, J. L. R. Watts, B. Harteneck, A. Scholl, A. Young, A. Doran, and Y. Suzuki, J. Appl. Phys. **109**, 07D712 (2011).
[16] A. P. Ramirez, J. Phy.-Condens. Matter **9**, 8171 (1997).

[17] J. M. D. Coey, M. Viret, and S. von Molnar, Adv. Phys. **48**, 167 (1997).
[18] L. C. Phillips, M. Ghidini, X. Moya, F. Maccherozzi, S. S. Dhesi, and N. D. Mathur, J. Phys. D **46**, 032002 (2013).
[19] D. Ruzmetov, Y. Seo, L. J. Belenky, D. M. Kim, X. Ke, H. Sun, V. Chandrasekhar, C.-B. Eom, M. S. Rzchowski, and X. Pan, Adv. Mater. **17**, 2869 (2005).
[20] Y. Takamura, R. V. Chopdekar, Y. Suzuki, A. Scholl, A. Doran, J. A. Liddle, and B. Harteneck, Nano Lett. **6**, 1287 (2006).
[21] M. Mathews, R. Jansen, G. Rijnders, J. C. Lodder, and D. H. A. Blank, Phys. Rev. B **80**, 064408 (2009).
[22] R. W. Schwartz, T. Schneller, and R. Waser, Compt. Rend. Chim. **7**, 433 (2004).
[23] I. Szafraniak, C. Harnagea, R. Scholz, S. Bhattacharyya, D. Hesse, and M. Alexe, Appl. Phys. Lett. **83**, 2211 (2003).
[24] X. Obradors, T. Puig, M. Gibert, A. Queraltó, J. Zabaleta, and N. Mestres, Chem. Soc. Rev. **43**, 2200 (2014).
[25] T. Okuno, K. Shigeto, T. Ono, K. Mibu, and T. Shinjo, J. Magn. Magn. Mater. **240**, 1 (2002).
[26] J. Zabaleta, M. Jaafar, P. Abellán, C. Montón, O. Iglesias-Freire, F. Sandiumenge, C. A. Ramos, R. D. Zysler, T. Puig, A. Asenjo, N. Mestres, and X. Obradors, J. Appl. Phys. **111**, 024307 (2012).
[27] J. Zabaleta, S. Valencia, F. Kronast, C. Moreno, P. Abellán, J. Gázquez, H. Sepehri-Amin, F. Sandiumenge, T. Puig, N. Mestres, and X. Obradors, Nanoscale **5**, 2990 (2013).
[28] M. Jaafar, J. Gomez-Herrero, A. Gil, P. Ares, M. Vázquez, and A. Asenjo, Ultramicroscopy **109**, 693 (2009).
[29] See supplementary material at http://dx.doi.org/10.1063/1.4891277 for MFM image of self-assembled LSMO nanoislands with different vortex core orientation and numerical simulations of the magnetization of different aspect ratio LSMO nanoislands under in-plane magnetic field.
[30] J. M. García-Martín, A. Thiaville, J. Miltat, T. Okuno, L. Vila, and L. Piraux, J. Phys. D **37**, 965 (2004).
[31] J. Raabe, R. Pulwey, R. Sattler, T. Schweinbock, J. Zweck, and D. Weiss, J. Appl. Phys. **88**, 4437 (2000).
[32] M. Jaafar, R. Yanes, D. Perez de Lara, O. Chubykalo-Fesenko, A. Asenjo, E. M. Gonzalez, J. V. Anguita, M. Vazquez, and J. L. Vicent, Phys. Rev. B **81**, 054439 (2010).
[33] L. D. Buda, I. L. Prejbeanu, M. Demand, U. Ebels, and K. Ounadjela, IEEE Trans. Magn. **37**, 2061 (2001).
[34] S. Agramunt-Puig, N. Del-Valle, C. Navau, and A. Sanchez, Appl. Phys. Lett. **104**, 012407 (2014).